Formation of ethane and propane via abiotic reductive conversion of acetic acid in hydrothermal sediments

Min Song[a,b,1,2], Florence Schubotz[a,b], Matthias Y. Kellermann[a,b,3], Christian T. Hansen[a,b], Wolfgang Bach[a,b], Andreas P. Teske[c], and Kai-Uwe Hinrichs[a,b,1]

[a]MARUM – Center for Marine Environmental Sciences, University of Bremen, Bremen D-28359, Germany; [b]Department of Geosciences, University of Bremen, Bremen D-28359, Germany; and [c]Department of Earth, Marine and Environmental Sciences, University of North Carolina at Chapel Hill, Chapel Hill, NC 27599-3300

Edited by Marilyn L. Fogel, University of California, Riverside, CA, and approved October 8, 2021 (received for review March 21, 2020)

A mechanistic understanding of formation pathways of low-molecular-weight hydrocarbons is relevant for disciplines such as atmospheric chemistry, geology, and astrobiology. The patterns of stable carbon isotopic compositions ($\delta^{13}C$) of hydrocarbons are commonly used to distinguish biological, thermogenic, and abiotic sources. Here, we report unusual isotope patterns of nonmethane hydrocarbons in hydrothermally heated sediments of the Guaymas Basin; these nonmethane hydrocarbons are notably ^{13}C-enriched relative to sedimentary organic matter and display an isotope pattern that is reversed relative to thermogenic hydrocarbons (i.e., $\delta^{13}C$ ethane > $\delta^{13}C$ propane > $\delta^{13}C$ *n*-butane > $\delta^{13}C$ *n*-pentane). We hypothesized that this pattern results from abiotic reductive conversion of volatile fatty acids, which were isotopically enriched due to prior equilibration of their carboxyl carbon with dissolved inorganic carbon. This hypothesis was tested by hydrous pyrolysis experiments with isotopically labeled substrates at 350 °C and 400 bar that demonstrated 1) the exchange of carboxyl carbon of C_2 to C_5 volatile fatty acids with ^{13}C-bicarbonate and 2) the incorporation of ^{13}C from ^{13}C-2–acetic acid into ethane and propane. Collectively, our results reveal an abiotic formation pathway for nonmethane hydrocarbons, which may be sufficiently active in organic-rich, geothermally heated sediments and petroleum systems to affect isotopic compositions of nonmethane hydrocarbons.

nonmethane hydrocarbons | hydrothermal sediments | volatile fatty acid | abiotic ethanogenesis | abiotic propanogenesis

Low–molecular weight (LMW) hydrocarbons (i.e., methane through pentane [C_1 to C_5]) are widespread in marine sediments (1–3) in which they may fuel chemosynthetic ecosystems or zones of intense microbial activity at or below the seafloor. Three principal sources exist for these compounds: biological processes that turn small carbon-bearing compounds into methane (4) and, in smaller quantities, its higher homologs (5), thermal cracking of kerogen and higher hydrocarbons (6), and abiotic production (7). Stable carbon isotopic compositions ($\delta^{13}C$) of LMW hydrocarbon are a powerful tool that aids in distinguishing these sources (8, 9). Likewise, carbon isotope patterns within the homologous series of LMW hydrocarbons have diagnostic values (*SI Appendix*, Fig. S1 *A–E*). That is, $\delta^{13}C$ values of thermogenic hydrocarbons, formed from thermal cracking of kerogen, increase with carbon number (e.g., refs. 10 and 11). By contrast, abiotic hydrocarbons formed via Fischer–Tropsch type (FTT) reduction of aqueous CO_2 (12) or from polymerization of methane (9) are increasingly depleted in ^{13}C with increasing carbon number, resulting in an inverse isotope trend compared to thermogenic production. Accordingly, methane formed via FTT reactions is typically isotopically enriched in ^{13}C (less negative $\delta^{13}C$ values) relative to thermogenic methane, while nonmethane hydrocarbons formed by polymerization of methane are substantially depleted in ^{13}C (more negative $\delta^{13}C$ values) relative to those formed by FTT reactions and thermogenic processes. Lastly, biogenic methane is generally ^{13}C-depleted relative to methane from other sources (4). For ethane and propane, a biological formation pathway involving the reduction of acetate was suggested (5). Volatile fatty acids (VFAs) are produced by thermal decomposition of sedimentary organic matter (13–16) and may accumulate to substantial levels in oil field waters (13, 17) and geothermally heated subsurface sediments (16, 18). Notably, VFAs may serve as potential substrates for the generation of C_{2+} hydrocarbons either via biological processes (5) or via abiotic decomposition involving decarboxylation and/or deformylation (19).

In this study, we investigated LMW hydrocarbons in 230 samples of both hydrothermally heated and cold sediments from the Guaymas Basin and observed unusual carbon isotope patterns for ethane, propane, *n*-butane, and *n*-pentane. We note that none of the above-described formation

Significance

Nonmethane, low-molecular-weight hydrocarbons are typically formed in geothermally heated subsurface sediments by cracking of larger precursor molecules. The Guaymas Basin serves as a sedimentary model system for extremely rapid formation of petroleum-like compounds. Here, C_2 to C_5 hydrocarbons are unusually enriched in ^{13}C, and their isotope pattern is distinct from that found in conventional petroleum systems, suggesting a different pathway for their formation. Using isotope tracer experiments at temperatures and pressures pertinent to hydrothermal conditions, we show that ethane and propane can be formed by reductive conversion of acetic acid, whose carboxylic group was isotopically equilibrated with the dissolved inorganic carbon pool. Our findings reveal a formerly unrecognized formation pathway for two major components in natural gas.

Author contributions: M.S., F.S., A.P.T., and K.-U.H. designed research; M.S., M.Y.K., and C.T.H. performed research; M.S., F.S., M.Y.K., A.P.T., and K.-U.H. analyzed data; M.S., K.-U.H., C.T.H., and W.B. designed the hydrothermal experiments; M.Y.K., A.P.T., C.T.H., and W.B. provided input to the paper; and M.S., F.S., and K.-U.H. wrote the paper.

The authors declare no competing interest.

This article is a PNAS Direct Submission.

[1]To whom correspondence may be addressed. Email: m.song@utoronto.ca or khinrichs@uni-bremen.de.

[2]Present address: Department of Earth Sciences, University of Toronto, 22 Ursula Franklin Street, Toronto, ON M5S 3B1, Canada.

[3]Present address: Institute for Chemistry and Biology of the Marine Environment, Carl von Ossietzky University Oldenburg, D-26382 Wilhelmshaven, Germany.

This article contains supporting information online at http://www.pnas.org/lookup/suppl/doi:10.1073/pnas.2005219118/-/DCSupplemental.

Published November 15, 2021.

pathways can satisfactorily explain the isotopic ordering of the nonmethane hydrocarbons observed in the hydrothermally impacted sediments of the Guaymas Basin (*SI Appendix*, Fig. S1*F*). The Guaymas Basin is a unique locality where rapid deposition of organic-rich sediments combined with hot basaltic sill intrusions into the unconsolidated sediments results in rapid heating of young, immature organic matter. This causes the generation of large amounts of complex petroleum-like compounds (20–24), LMW hydrocarbons (25, 26), VFAs (27), and ammonia (28), which migrate upwards with the hydrothermal fluids to fuel a flourishing seafloor ecosystem (29, 30).

Given the unusual isotope patterns of C_2 to C_5 hydrocarbons, we explored the potential for an alternative formation pathway involving reductive conversion of VFAs and prior equilibration of their carboxyl groups with ambient dissolved inorganic carbon (DIC). Thus, we conducted sequential hydrous pyrolysis experiments amended with ^{13}C-labeled DIC and acetate to assess whether this pathway can produce and explain the observed isotope pattern.

Results and Discussion

Push core samples were retrieved from Guaymas Basin sediments at 11 different sites, spanning temperatures from 3 °C at the sediment surface to 180 °C at 40 to 50 centimeters below the seafloor (*SI Appendix*, Table S1 and Figs. S2 and S3). Except for the off-axis site Octopus Mound located at the central seep (31, 32), the remaining 10 research sites were located in the southern trough, which were hydrothermally highly active (33). While most of these sites were clustered within ∼500-m distance, Northern Tower Site 2 and Site 3 were located further north in the trough (32). At all sites, we observed high amounts of LMW hydrocarbons (Dataset S1).

Microbial Overprint of Isotopic Compositions from Deeply Sourced LMW Hydrocarbons. A large fraction of the LMW hydrocarbons is formed in the deep subsurface, where basaltic sill intrusions result in thermogenic degradation of immature organic matter (26). The $\delta^{13}C$ values from samples obtained in the temperature range of ∼150 to 180 °C are characteristic of these deeply sourced hydrocarbons, because these samples have presumably not been impacted by biological processes, as observed in colder sediments (Fig. 1). At these high temperatures, methane carried a typical thermogenic signal (−42.8 ± 0.4‰, mean ± SD, and $n = 8$), consistent with methane $\delta^{13}C$ values reported at deeply buried sills (34). However, the C_2 to C_5 hydrocarbons exhibited unusual ^{13}C enrichments and an isotope pattern that conforms to neither a traditional thermogenic origin nor a known abiotic production pathway (cf. *Unusual Isotope Pattern for LMW Hydrocarbons in the Guaymas Basin*).

At in situ temperatures of 3 to 60 °C, vigorous microbial activity is commonly observed in Guaymas Basin sediments (35). Within this temperature range, $\delta^{13}C_1$ values spanned a wide range from −81.7 to −7.5‰ (Fig. 1). The most-negative values strongly suggest the activity of biological methanogenesis, while the least negative values probably result from the activity of anaerobic methane-oxidizing communities in cooler surface sediments (cf. refs. 35–37). The microbially sourced admixtures of methane are also indicated by the abundance ratios of $C_1/(C_2+C_3)$ (2). At the central seep site Octopus Mound, where in situ temperatures in the sediment core did not exceed 3 °C, $C_1/(C_2+C_3)$ ratios (319 ± 137, mean ± SD, and $n = 24$) and relatively negative $\delta^{13}C_1$ values (−81.7 to −55.3‰) indicate admixtures of methane from microbial sources (32) (Dataset S1). Likewise, $\delta^{13}C$ of nonmethane hydrocarbons showed notable, mostly positive, deviations from the deeply sourced values observed at temperatures above 150 °C.

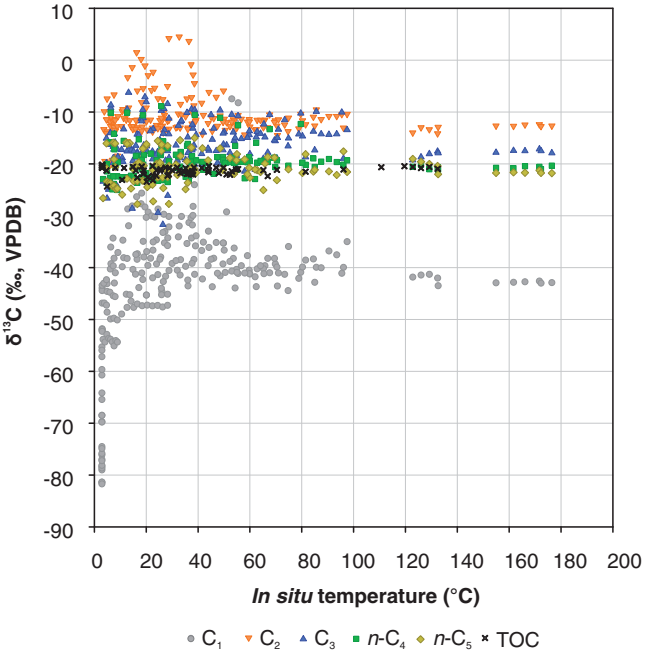

Fig. 1. Carbon isotopic compositions ($\delta^{13}C$) of C_1 to C_5 hydrocarbons and TOC in a wide range of in situ temperatures at the Guaymas Basin. Samples were retrieved from Guaymas Basin sediments at 11 different sites (*SI Appendix*, Table S1). Data from a small fraction of samples (11 out of 230) were published previously (43) (Dataset S1).

For example, $\delta^{13}C_2$, $\delta^{13}C_3$, $\delta^{13}C_4$, and $\delta^{13}C_5$ reached respective values as high as +4.5‰, −6.3‰, −8.9‰, and −15.0‰ (Fig. 1). We attribute these deviations to isotopic fractionation induced by biologically mediated oxidation, consistent with the presence and activity of hydrocarbon-oxidizing microbes in the shallower hydrothermally warmed sediments of the Guaymas Basin (38–40), including anaerobic methane-oxidizing communities (e.g., refs. 36, 37, and 41). Although ethane is presumed to be the most chemically inert LMW hydrocarbon under anaerobic conditions with retarded microbial utilization (42), extraordinary ^{13}C-enriched ethane values of up to +4.5‰ at one sediment core (4484-6) from the Mat Mound site, which is situated below 40 °C, are suggestive of microbial oxidation as prominent process (43). Indeed, microbial anaerobic oxidation of ethane, propane, and *n*-butane takes place under sulfate-reducing conditions at mesophilic to thermophilic temperatures (38–40, 43–46) as found in the Guaymas Basin.

Unusual Isotope Pattern for LMW Hydrocarbons in the Guaymas Basin. Above 80 °C, which has been proposed as the upper thermal limit for hydrocarbon-degrading microbes in subsurface hydrocarbon reservoirs (47), $\delta^{13}C_1$ values exhibited a narrower range between −43.5 and −35.0‰ and $C_1/(C_2+C_3)$ ratios were between 5.5 and 81.9 (Fig. 1 and Dataset S1). This trend points to a diminished impact of microbial processes and to a predominantly thermogenic origin of methane at these elevated temperatures, as reported previously (34). In addition, $\delta^{13}C$ values for the nonmethane hydrocarbon were relatively uniform compared to those at lower temperatures. In particular, $\delta^{13}C$ values of propane and ethane ranged between −19.3‰ to −9.6‰ and thus were enriched in ^{13}C relative to total organic carbon (TOC) values ($\delta^{13}C_{TOC}$: −21.5‰ to −20.6‰) (Fig. 1).

We defined the mean isotopic compositions of hydrocarbons detected in samples with in situ temperatures >80 °C as hydrothermal endmember values, which are only minimally impacted

by microbial processes. The averaged values for samples above 80 °C were −40.8 ± 2.3‰ (mean ± SD and n = 23) for methane, −12.1 ± 1.2‰ (mean ± SD and n = 23) for ethane, −15.9 ± 2.9‰ (mean ± SD and n = 23) for propane, −19.9 ± 1.8‰ (mean ± SD and n = 21) for n-butane, and −20.9 ± 1.4‰ (mean ± SD and n = 19) for n-pentane. While $\delta^{13}C_1$ values indicate a predominant thermogenic source for methane (34), the isotope pattern of C_{2+} hydrocarbons is reversed relative to that of the conventional thermogenic hydrocarbons (*SI Appendix*, Fig. S1 *A* and *F*).

Similar reversed isotope patterns for C_{2+} hydrocarbons have been reported in other geologic settings and were explained as a result of, for example, FTT reactions (12) or methane polymerization (*SI Appendix*, Fig. S1 *B* and *C* and ref. 9). Alternatively, subsurface mixing of LMW hydrocarbons generated from kerogen with those generated by secondary cracking of oil and condensate (48) or other processes could result in anomalously ^{13}C-enriched hydrocarbons. While we cannot rule out the aforementioned processes, none of these scenarios satisfactorily explains the isotopic and compositional patterns observed in this study as discussed in detail in the supporting text (*SI Appendix*). In brief, $\delta^{13}C_1$ values are substantially lower than those predicted for FTT reactions, and nonmethane hydrocarbons formed via methane polymerization would be depleted in ^{13}C relative to methane (49). Moreover, in the organic-rich setting of the Guaymas Basin, which serves as a model for the rapid thermal degradation of organic matter, it is unlikely that reduction of CO_2 via FTT reactions constitutes the predominant pathway of hydrocarbon formation.

In line with the geological requirements that support the subsurface mixing scenario (48), the LMW hydrocarbons in our samples probably represent mixtures of products that were formed over a wide range of temperatures and sediment depths. Because of the high heat flow and the hydrothermal circulation, the generation, expulsion, and migration of hydrocarbons occurred nearly simultaneously on millennial timescales (e.g., ref. 50). While we cannot rule out secondary cracking reactions, it is unlikely that these have exerted major control on the isotopic composition of LMW hydrocarbons in the dynamic system of Guaymas Basin. This view is supported by the absence of negative correlations between δ^{13}C values of ethane and propane and their abundance ratios relative to higher hydrocarbons (*SI Appendix*, Fig. S4 *D* and *E*). In addition to thermolytic cracking reactions, the oxidation of hydrocarbons could result in ^{13}C enrichment of the residual hydrocarbon pool. While the microbially mediated oxidation of LMW hydrocarbons is presumably irrelevant at temperatures >80 °C (35, 47), abiotic oxidation may have resulted in such ^{13}C enrichment of ethane and propane, as previously suggested for the Main Endeavor Field at the Juan de Fuca Ridge (51). Indeed, the positive correlation between $C_1/(C_2+C_3)$ ratios and δ^{13}C values of ethane and propane for samples situated at temperatures >80 °C (*SI Appendix*, Fig. S4 *B* and *C*) may hint at a potential role of abiotic oxidation of ethane and propane. However, no straightforward picture emerges based on isotopic compositions, relative distributions, and the absolute concentrations of C_{2+} hydrocarbons (*SI Appendix*, Supplementary Text and Dataset S1) regarding the relevance of abiotic oxidation for shaping the isotope patterns of LMW hydrocarbons. Finally, the scenario of ethane and propane being produced from strongly ^{13}C-enriched, highly mature kerogen appears unlikely given that sedimentary kerogen in the deep subsurface of Guaymas Basin is not conspicuously ^{13}C-enriched (52). Moreover, strong ^{13}C enrichment is only observed in highly metamorphosed organic matter with H/C ratios below 0.1 (53) (i.e., values probably incompatible with a significant potential of hydrocarbon production). Therefore, some additional sources for the HMW hydrocarbons are required to satisfactorily explain their isotopic compositions and isotope reversal in our samples.

Experimental Evidence for *n*-Alkane Synthesis through Reductive Conversion of Acetic Acid. As no known pathways and mechanisms provide a conclusive explanation for the unusual isotope signatures in LMW hydrocarbons at the Guaymas Basin, we considered an alternative mechanism involving the reductive conversion of VFAs to n-alkanes as potential mechanism to generate C_2 to C_{2+n} hydrocarbons with the observed isotope pattern. The reason for considering such a mechanism is a similarly reversed isotope pattern in the series of VFAs, from acetic acid through valeric acid, in oil field waters of the San Joaquin Basin (54); this isotope pattern resembled that of the corresponding hydrocarbons in our study (Fig. 2). In that study, the δ^{13}C values in the acid components increased with decreasing molecular weight and were generally higher than their syngenetic oils (54), in analogy to the isotopic enrichment of ethane, propane, n-butane, and n-pentane relative to TOC observed in our samples. The authors suggested that exchange of the carboxylic carbon of VFAs and the isotopically heavier DIC was the cause of ^{13}C enrichment in the acid (54) and provided additional supporting evidence by hydrous pyrolysis of oil-prone source rocks (55).

We consequently explored whether reductive conversion of VFAs may act as alternative formation pathway for LMW hydrocarbons within the hydrothermal sediments of the Guaymas Basin. In conjunction with an isotopic equilibration of the carboxylic acid carbon and ambient DIC, reductive conversion of VFAs would result in isotopically heavy C_2 to C_5 hydrocarbons and a reversed isotope pattern. Both the high abundance of VFAs (27) and H_2-rich hydrothermal fluids (3, 56, 57) in the Guaymas Basin provide favorable conditions for these reactions. Gibbs free-energy computations further indicate that reduction of acetic acid to ethane is thermodynamically favorable under environmental conditions pertinent to the Guaymas Basin subsurface (*SI Appendix*, Fig. S6). These reactions probably take place in the subsurface in the vicinity of sill intrusions at substantially higher temperatures than those observed in the sampled shallow cores. This is consistent with the ^{14}C dating of petroleum-like compounds and methane in the Guaymas Basin, which place the reaction zone at no greater than about 10- to 30-m sediment depth for petroleum and at least 50 m for methane (23, 58) in the Guaymas Basin.

In order to test the hypothesis involving isotopic equilibration of carboxylic carbon with DIC followed by reductive conversion of VFAs to hydrocarbons at high temperatures, we conducted four hydrous pyrolysis experiments (Table 1; hereafter referred as Exp. I, II, III, and IV). We designed these experiments primarily to demonstrate the feasibility of the pathway and to optimize yields of products without attempting to simulate in situ conditions. For this, we mixed warm hydrothermal sediment retrieved from the temperate hydrothermal mat area sampled during Alvin dive 4861 (core 4861–36) (32) (*SI Appendix*, Table S1) with artificial seawater (59) (see *Materials and Methods*) at an initial fluid/sediment ratio of 7 to 11 and heated the mixture to 350 °C at 400 bars. In Exp. I, the mixture was amended with ^{13}C-labeled bicarbonate (~9,300‰) and unlabeled VFAs (acetic acid through n-valeric acid, with δ^{13}C between −40 and −20‰). After 24 h, we observed highly ^{13}C-labeled VFAs ranging from 209 to 979‰, while $\delta^{13}C_{DIC}$ dropped to ~2,400‰ (Fig. 3*A* and *SI Appendix*, Table S2). Isotope exchange of carboxylic carbons of VFAs and DIC proceeded rapidly, forming a reversed isotope pattern for VFAs (Fig. 3*A*). This observation is in accordance with the proportionally decreasing contribution of ^{13}C-enriched carboxylic carbon in VFA with increasing carbon chain length. This experimental result confirms an exchange of carboxylic carbon between VFAs and DIC under hydrothermal conditions (Eq. 1 in Fig. 4).

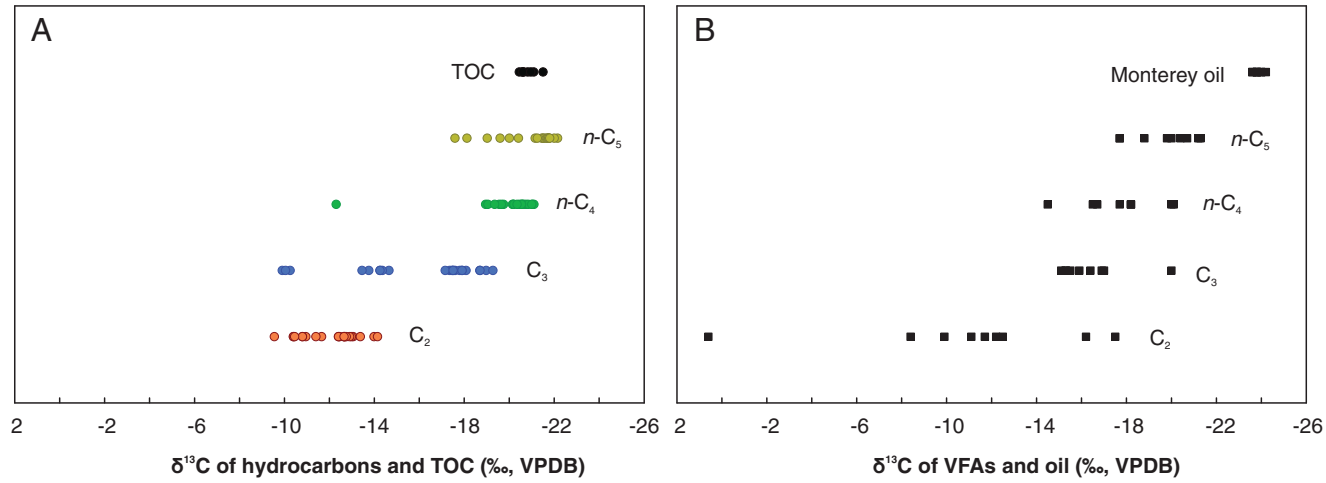

Fig. 2. Comparison of isotopic patterns of C_2 to C_5 hydrocarbons from the Guaymas Basin and the corresponding VFAs in oil field waters from the San Joaquin Basin. (*A*) $\delta^{13}C$ values of nonmethane hydrocarbons, ethane through *n*-pentane (C_2 to C_5), and TOC at Guaymas Basin in this study at in situ temperatures >80 °C. Data were collected from 23 samples of the following sampling sites: T-logger mat/Marker 14, Megamat, INSINC (in situ incubator) Mat I, and Cathedral Hill/Marker 24 in which in situ temperatures were >80 °C (Dataset S1). (*B*) $\delta^{13}C$ values of VFAs, acetic acid through *n*-valeric acid (C_2 to C_5), and their coproduced oil from oil field waters of the San Joaquin Basin at temperatures of 96 to 135 °C. Data were taken from ref. 54.

In experiments II through IV, the basic setup and sediment material was identical to Exp. I, but label was introduced via addition of ^{13}C-2-sodium acetate (ca. 4,000‰), and reducing conditions were established by addition of either 10 mM (Exp. II) or 100 mM (Exp. III and IV) of sodium formate (Table 1 and ref. 60). We designed these experiments to verify the transfer of the acetic acid–derived methyl carbon atom into ethane and possibly its higher homologs. In Exp. IV, sulfate was excluded from the artificial seawater to enhance the reducing power, resulting in the highest-H_2 concentration (Table 1 and *SI Appendix*, Table S3). We will primarily focus our discussion on the contrasting results of Exp. II and IV, which represent moderately versus strongly reducing conditions, respectively. In both experiments, we detected the formation of ^{13}C-enriched ethane, with $\delta^{13}C$ values ranging from 3.1‰ to 25.3‰ in Exp. II and from 31.4‰ to 78.3‰ in Exp. IV after 72 and 240 h (Fig. 3*B* and *SI Appendix*, Table S3). Surprisingly, we also observed ^{13}C-enriched propane whose $\delta^{13}C$ values were higher than those of ethane in both experiments, ranging from 12.7‰ to 56.4‰ (Exp. II) and from 118‰ to 261‰ (Exp. IV) after 72 to 240 h (Fig. 3*B* and *SI Appendix*, Table S3). Both ethane and propane were more ^{13}C-enriched in Exp. IV, in which reducing conditions were stronger, suggesting the presence of a reductive pathway involving acetic acid and other intermediates (Fig. 3*B*). Importantly, incorporation of the ^{13}C label in C-3 compound propane suggests that acetic acid must undergo other reactions in addition to its mere reduction.

Table 1. Initial concentrations (millimoles/liter fluid) of aqueous species and measured H_2 in Exp. I through IV

Components	Exp. I	Exp. II	Exp. III	Exp. IV
^{13}C-DIC (10% labeled)	14.4	—	—	—
DIC	—	—	2.8	1.1
^{13}C-2-Acetic acid (10% labeled)	—	21	22	29
Formic acid	—	11	103	136
Acetic acid	1.0	—	—	—
Propionic acid	0.7	—	—	—
n-Butyric acid	0.8	—	—	—
n-Valeric acid	0.3	—	—	—
SO_4^{2-}	27	27	28	4.8
*H_2	0.05	0.03	12	23

Experiments were conducted at 250 °C (in the first 24 h of Exp. II) to 350 °C and 400 bars. Refer to SI Appendix, Tables S2 and S3 for details. *H_2 concentration in Exp. I after 120 h and in Exp. II, III and IV after 72 h.

In the employed analytical window comprising LMW hydrocarbons and other LMW and water-soluble components, we identified potential intermediates based on their incorporation of ^{13}C label. These were the C-2 compound ethene and the two C-3 compounds acetone and propene, all of which were more strongly labeled than the products ethane and propane (Fig. 4 and *SI Appendix*, Table S3). The formation of ^{13}C-enriched ethene is consistent with a stepwise reduction of acetic acid, possibly in analogy to the proposed stepwise reduction of formic acid to methane under hydrothermal conditions (61). Accordingly, the putative intermediate ethene could, for example, result from reduction of acetic acid to ethanol (62) and subsequent dehydration (Eq. 2 in Fig. 4). The presence of strongly ^{13}C-labeled C-3 compounds such as acetone and propene, with $\delta^{13}C$ values of up to ~1,300‰ and ~800‰, respectively (*SI Appendix*, Table S3), calls for a mechanism involving the fusion of two acetic acid molecules. Indeed, acetone can be formed from reaction of two molecules of acetic acid through bimolecular ketonization on surfaces of zeolites and metal oxides such as MgO and MnO_2 (63). The ketonization process may involve reactions of highly reactive methide anions from thermal decarboxylation of acetic acid (e.g., refs. 64 and 65). Consequently, the methyl groups from two molecules of acetic acid (^{13}C labeled in our experiments) are translated into the methyl groups of the acetone (63). The relatively low $\delta^{13}C$ values for acetone in comparison to acetic acid suggests that additional reactions independent of acetic acid as reactant contribute to the acetone pool. Subsequently, ^{13}C-enriched propene could be formed from hydrogenation of ^{13}C-enriched acetone to 2-propanol followed by dehydration (e.g., ref. 66). Eventually, hydrogenation of ^{13}C-enriched propene results in ^{13}C-enriched propane. These partial reactions, which are consistent with the identified ^{13}C-labeled intermediates and products, are summarized in net Eq. 3 (Fig. 4). This mechanism is further supported by a positive correlation between natural $\delta^{13}C$ values of propane and ethane and a good fit between predicted and natural $\delta^{13}C_3$ values versus natural $\delta^{13}C_2$ (*SI Appendix*, Fig. S7).

We note that in the two relatively oxidizing Experiments II and III, we have also detected ^{13}C-labeled propionic acid (*SI Appendix*, Table S3). While its presence is not fully conclusive,

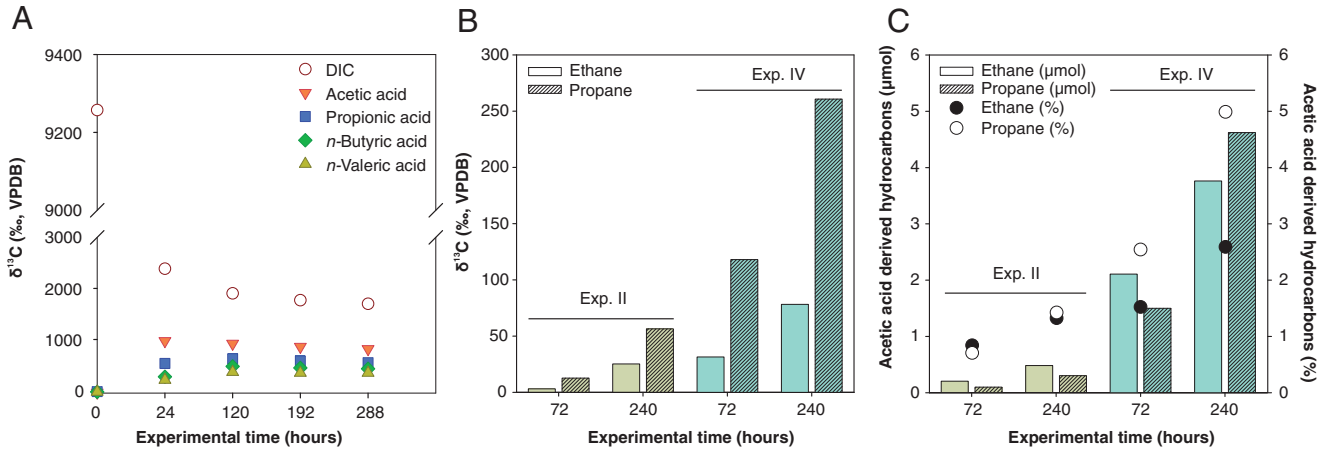

Fig. 3. Results from hydrous pyrolysis experiments with Guaymas Basin sediments after addition of ^{13}C-labeled tracers. (*A*) δ^{13}C values of DIC and VFAs (acetic acid through valeric acid) during Exp. I with an addition of 10% ^{13}C-labeled DIC (9257‰) and unlabeled VFAs. δ^{13}C values of ethane and propane (*B*) and molar yields and percentage of ethane and propane (*C*) that incorporated ^{13}C label from ^{13}C-2–acetic acid (4,554‰ and 4,357‰, respectively) in Exp. II and Exp. IV after 72 to 240 h (calculated according to the stoichiometry of Eqs. 2 and 3 in Fig. 4). Refer to Table 1 for the experimental conditions.

it is consistent with the above-mentioned mechanism. Since 1-propanol is a byproduct of the acid-catalyzed dehydration of 2-propanol (67), the detected ^{13}C-labeled propionic acid could then originate from oxidation of 1-propanol in the experiments with higher seawater sulfate levels, at which increasingly oxidizing conditions were established after the release of H_2 from formic acid had ceased. Alternatively, a fraction of propionic acid may also be formed from oxidative degradation of ^{13}C-labeled alkenes detected in these experiments (e.g., ref. 68). Other side products include ^{13}C-enriched methane, formed from decarboxylation of acetic acid under high temperature in all experiments (19), and an increase of ^{13}C enrichment of DIC in Exp. II, resulting from enhanced oxidation of acetic acid in this experiment (19). Aside from C-1 to C-3 products, we have also detected strongly ^{13}C-labeled butene and pentene in the Experiments III and IV (*SI Appendix*, Table S3). Although their formation pathway can only be resolved with targeted experiments involving other ^{13}C-labeled reactants, an analogous set of reactions involving propagation of reactive methide anions and reduction reactions is conceivable.

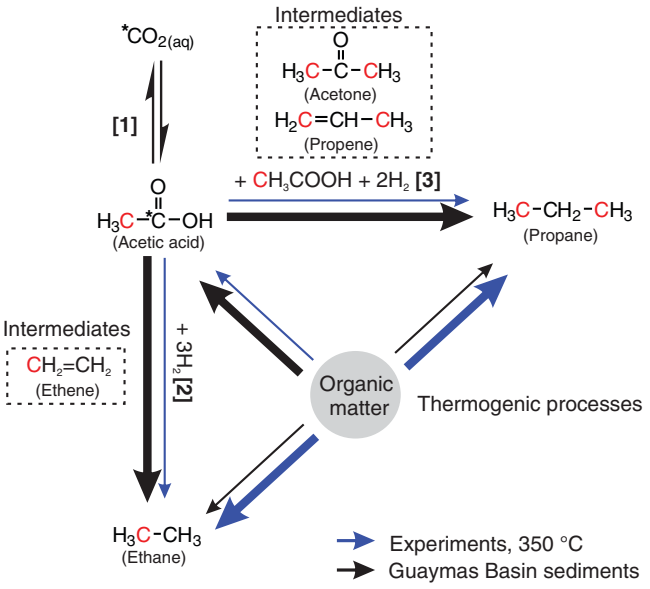

Fig. 4. Reaction scheme for the formation of ethane and propane from acetic acid. The relative contributions of hydrocarbon generation via acetic acid conversion versus thermogenic degradation of organic matter under laboratory (blue) and natural conditions (black) are visualized by different thicknesses of arrows; thicker lines indicate higher production under the corresponding conditions. Carboxyl carbon (indicated with *) exchange reaction is indicated by Eq. 1, and pathways for ethane and propane formed from conversion of acetic acid and the corresponding reaction intermediates are indicated by Eqs. 2 and 3, in which carbon atoms originating from $^{13}C_2$–acetic acid in the experiments are highlighted in red.

The low ^{13}C enrichment in ethane and propane relative to the ^{13}C content of the acetic acid pool (δ^{13}C of ~4,000‰) suggests that under the experimental conditions, the major fraction of both hydrocarbons is derived from unlabeled precursors associated with the immature sedimentary organic materials. However, the increasing accumulation of ^{13}C label in hydrocarbons over the course of the experiment indicates progressive transfer of the acetic acid's methyl carbon into these compounds (Fig. 3*B*). Mass–balance constraints (see *Materials and Methods*) suggest that acetic acid–derived hydrocarbons increased with time and accounted for ~1 to 3% of total ethane and 1 to 5% of total propane in Exp. II and IV after 72 to 240 h of heating (Fig. 3*C* and *SI Appendix*, Fig. S8). We note that the relative production rates of hydrocarbons from unlabeled versus labeled precursors have influenced the differences in relative yields of acetic acid–derived ethane and propane in the respective hydrocarbon pools, as illustrated by the comparatively similar molar yields of ethane and propane (Fig. 3*C*).

The proposed reaction pathways involving retention of one acetic acid–derived aliphatic carbon atom in ethane and two acetic acid–derived aliphatic carbon atoms in propane are consistent with the natural isotopic compositions of these hydrocarbons in the Guaymas Basin. Accordingly, because of the equilibration of the carboxylic carbon of the acetic acid with relatively ^{13}C-enriched ambient DIC in the hot Guaymas Basin subsurface (Eq. 1 in Fig. 4), the conversion of acetic acid will result in stronger ^{13}C enrichment in the C-2 products compared to the C-3 products. By analogy, reductive conversion of propionic acid and longer-chain VFAs could similarly contribute to the formation of propane and higher hydrocarbons *n*-butane and *n*-pentane, but dedicated experiments with the respective reactants are required for verification. Accordingly, the observed isotope patterns of LMW hydrocarbons in Guaymas Basin sediments could reflect the predominant accumulation of hydrocarbons generated via reactions of acetic acid and its higher homologs rather than via thermogenic degradation of organic matter (Fig. 4). A possible reason could be the rapid

transfer of thermally immature sedimentary organic matter into the oil window.

Collectively, our results indicate a formation mechanism involving carboxyl carbon exchange of acetic acid followed by its abiotic reductive conversion to nonmethane LMW hydrocarbons in reducing hydrothermal sediments. In such a system, ongoing hydrothermal decomposition of sedimentary organic matter results in significant generation of organic acids, which incorporate inorganic carbon through rapid carbon exchange with DIC at high temperatures. Continuous reductive conversion of organic acids to nonmethane hydrocarbons then ultimately results in the unusual systematic isotope pattern observed at the Guaymas Basin. While conventional thermogenic LMW hydrocarbons may account for a proportion of the hydrocarbon pool, their isotopic signals appear to be overprinted by these reductive processes. It is conceivable that this process also occurs in other similar sedimentary systems; thus, its effects on isotopic compositions of nonmethane hydrocarbons should be taken into consideration.

Materials and Methods

A total of 21 push cores were collected for hydrocarbon analysis from hydrothermally active and inactive sediments by deep-sea submersible Alvin at 11 sites (*SI Appendix*, Table S1) during three expeditions conducted by the R/V Atlantis in the Guaymas Basin in 2008, 2009, and 2016. Before sampling, temperature profiles at each sampling site were recorded using Alvin's external heat-flow probe, as described elsewhere (69).

LMW Hydrocarbons. Volumes of 2 to 5 mL of fresh sediment were taken within 4 h after core recovery by a head-cut syringe in 2-cm intervals and placed in headspace vials containing 5 mL of 1 M NaOH solution, crimp sealed with butyl rubber septa, and stored upside down at −20 °C for further analysis. Mixtures in headspace vials were homogenized by gently shaking overnight in room temperature. Concentrations of LMW hydrocarbons were defined by Trace gas chromatography (GC) equipped with a flame ionization detector. A carboxen 1006 PLOT column (30 m × 0.32 mm, SUPELCO) was equipped for analysis of methane with temperature set at 40 °C (held for 6 min). A AT-Q column (30 m × 0.32 mm, Alltech) was applied for the analysis of C_2 to C_5 higher alkanes, with a temperature program of 60 °C (held for 1 min) to 240 °C (held for 7 min) at a rate of 40 °C/min. The molar fraction of LMW hydrocarbons was calculated by injection of known quantities of hydrocarbon gas standards (Air Liquide). It should be noted that since the push cores were not collected in gas-tight sampling devices, degassing of volatiles is unavoidable in gas-rich porewater. Because of the higher volatility of methane relative to ethane and propane, $C_1/(C_2+C_3)$ values reported here are minima.

The determination of stable carbon isotope ratios of LMW hydrocarbons was performed by GC coupled to Delta Plus XP isotope ratio mass spectrometer (GC-IRMS) via a combustion interface-III (all from Thermo Finnigan GmbH). The applied column and temperature program were identical to those for the concentration measurements. The internal precision was ±0.5‰. Stable carbon isotope ratios were reported in $\delta^{13}C$ notation (per mil, ‰) relative to the Vienna Peedee Belemnite Standard (VPDB), with $\delta^{13}C = (R_{sample}\text{-}R_{VPDB})/R_{VPDB} \times 10^3$, where $R = {}^{13}C/{}^{12}C$ and $R_{VPDB} = 0.0112372 \pm 2.9 \times 10^{-6}$. The precision of the gas measurements was evaluated by replicate injections of hydrocarbon gas standards (Air Liquide). The average $\delta^{13}C$ values for the standard gas mixtures were $\delta^{13}C_1 = -39.9 \pm 0.02$‰ (mean ± SD and $n = 3$), $\delta^{13}C_2 = -29.2 \pm 0.29$‰ (mean ± SD and $n = 3$), $\delta^{13}C_3 = -31.6 \pm 0.18$‰ (mean ± SD and $n = 3$), $\delta^{13}C_4 = -33.1 \pm 0.18$‰ (mean ≥ SD and $n = 3$), and $\delta^{13}C_5 = -27.9 \pm 0.17$‰ (mean ± SD and $n = 3$). $\delta^{13}C$ values were not reported in cases in which the concentrations were below the instrumental detection limit (e.g., peak area of $CO_2 < 0.5$ Vs) converted from hydrocarbons on GC-IRMS, corresponding to a concentration of ∼4 μmol C/L sediment porewater. Precision and accuracy of the instrument is regularly tested with standards.

Porewater Geochemistry. Porewater was obtained by Rhizon samplers at 1-cm intervals upon core retrieval onboard. Samples for VFA analysis were stored at −20 °C. For DIC analysis, 2-mL vials were completely filled with porewater and stored upside down at 4 °C until analysis. The concentration and $\delta^{13}C$ values of VFAs were analyzed onshore by isotope ratio monitoring liquid chromatography/mass spectrometry as described previously (70). The internal precision was <1‰. Carbon isotopic compositions of DIC were defined using a Delta Ray Isotope Ratio Infrared Spectrometer (IRIS) equipped with Universal Reference Interface Connect and autosampler (Thermo Fisher Scientific), as described previously (71). The internal precision was <0.2‰.

TOC. A total of ∼1 g of freeze-dried sediment was decalcified and analyzed with continuous-flow elemental analyzer–isotope ratio mass spectrometer for the content and isotopic compositions of TOC. The internal precision is ±0.1‰.

Hydrous Pyrolysis Experiments. Four hydrous pyrolysis experiments (Exp. I, II, III, and IV) were conducted using a customized Dickson-type flexible reaction cell setup (Parr Instruments) with no vapor present. Sediments from core 4861–36 were used: 20 to 25 g sediments with initial porewater/sediment mass ratio of ∼1:1 in Exp. I through III and 7 g freeze-dried materials in Exp. IV. A total of ∼70 to 80 g of artificial seawater (cf. ref. 59; sulfate and Mg were excluded in Exp. IV) were transferred with sediments into a gold reaction cell (V_{total} ∼ 100 mL), resulting in an initial fluid/sediment ratio of 7 to 11. Pressure in all experiments were set to 400 bars. Temperature was set to 350 °C, with the exception that in Exp. II, the temperature was set at 250 °C for first 24 h before elevated to 350 °C. Experiments were performed for a total of 288 h (Exp. I), 408 h (Exp. II), 72 h (Exp. III), and 240 h (Exp. IV). Fluid sample was taken to fill up a 1.5-mL vial and stored upside down at 4 °C for DIC concentration and isotopic composition measurement. DIC isotopic compositions were not measured for the Exp. IV due to the shutdown of IRIS; instead, CO_2 isotopic compositions in the corresponding samples were measured with GC-IRMS. A total of ∼1 mL of fluid was taken for VFA concentration and isotopic composition measurements. In addition, samples for LMW hydrocarbon concentration and isotopic composition measurements were stored in headspace vials, which were preflushed with N_2 and sealed with butyl rubber septa. For this, 1 to 2 mL of fluid were taken from the reaction cell into a 5-mL gas-tight syringe. With a freely moveable plunger, the fluid sample and the gas phase unmixing from the fluid upon depressurization were allowed to equilibrate (expand) to ∼1 atm within the closed syringe. Then, a volume of N_2 equal to the total volume within the syringe (fluid + unmixed gas) was drawn from the headspace vial to avoid overpressure, prior to transferring the contents of the syringe into the headspace vials. The instrumental methods are the same as described before. Between 1 and 2.5 mL of fluid were taken for H_2 concentration measurements; after equilibration between fluid and headspace, gas in headspace of a 5-mL syringe was directly injected to a GC equipped with thermal conductivity detector.

Isotopic Mass–Balance Calculations. In the isotopic mass–balance calculations, ethane and propane produced in the experiments are considered a mixture of products from reduction of ^{13}C-2–acetic acid and through thermal decomposition of sedimentary organic matter. The $\delta^{13}C$ values of hydrocarbons are estimated using a two-source, endmember-mixing approach (cf. ref. 72):

$$I_{HC} = f_{sed} \times I_{sed} + f_{Ac} \times I_{Ac}, \quad [1]$$

$$f_{sed} + f_{Ac} = 1, \quad [2]$$

where I_{HC} is measured $\delta^{13}C$ value for hydrocarbon at different experimental time points. I_{sed} is measured $\delta^{13}C$ value for thermogenic gas obtained from Exp. I during which no artificially reducing conditions were established; consequently, the released gases are assumed to be predominantly of thermogenic origin. I_{Ac} is $\delta^{13}C$ value of acetic acid at the beginning of each experiment. f_{sed} and f_{Ac} are the mass fraction contributions from thermogenic gas and gas from acetic acid reduction; therefore, f_{Ac} is used to estimate the molar concentration of hydrocarbons derived from reductive conversion of acetic acid.

Data Availability. All study data are included in the article and/or supporting information. Previously published data were used for this work (43, 73).

ACKNOWLEDGMENTS. We are grateful to the captain and crew of research vessel (R/V) *Atlantis* and the Human Occupied Vehicle (HOV) *Alvin* team for their expert support and the scientific party for sample recovery and documentary of *Alvin* dives during the cruise AT15-40, AT15-56 and AT37-06 funded by NSF (OCE-0647633 and OCE-1357238). We thank Jenny Wendt and Xavier Prieto-Mollar for their substantial technical support throughout the project, Heidi Taubner and Jessica Arndt for their assistance in DIC isotope measurements, Silvana Pape for measuring DIC concentrations for Exp. IV, Gunter Wegener and Karen G. Lloyd for providing the sulfate data, and Alexander Diehl for helping with H_2 gas analysis. This study was supported by Germany's Excellence Strategy—EXC-2077—390741603. M.S. was sponsored by the China Scholarship Council (CSC) and the Bremen International Graduate School for Marine Sciences (GLOMAR). A.P.T. acknowledges a fellowship of the Hanse Institute of Advanced Studies in Delmenhorst, Germany. We greatly appreciate the constructive comments and suggestions from the editor and three anonymous reviewers.

1. G. E. Claypool, K. A. Kvenvolden, Methane and other hydrocarbon gases in marine sediment. *Annu. Rev. Earth Planet. Sci.* **11**, 299–327 (1983).
2. B. B. Bernard, J. M. Brooks, W. M. Sackett, Natural gas seepage in the Gulf of Mexico. *Earth Planet. Sci. Lett.* **31**, 48–54 (1976).
3. J. Welhan, J. Lupton, Light hydrocarbon gases in Guaymas Basin hydrothermal fluids: Thermogenic versus abiogenic origin. *AAPG Bull.* **71**, 215–223 (1987).
4. M. J. Whiticar, E. Faber, M. Schoell, Biogenic methane formation in marine and freshwater environments: CO_2 reduction vs. acetate fermentation—Isotope evidence. *Geochim. Cosmochim. Acta* **50**, 693–709 (1986).
5. K.-U. Hinrichs *et al.*, Biological formation of ethane and propane in the deep marine subsurface. *Proc. Natl. Acad. Sci. U.S.A.* **103**, 14684–14689 (2006).
6. B. P. Tissot, R. Pelet, P. Ungerer, Thermal history of sedimentary basins, maturation indices, and kinetics of oil and gas generation. *AAPG Bull.* **71**, 1445–1466 (1987).
7. G. Etiope, M. Schoell, Abiotic gas: Atypical, but not rare. *Elements* **10**, 291–296 (2014).
8. M. J. Whiticar, Carbon and hydrogen isotope systematics of bacterial formation and oxidation of methane. *Chem. Geol.* **161**, 291–314 (1999).
9. B. Sherwood Lollar, T. D. Westgate, J. A. Ward, G. F. Slater, G. Lacrampe-Couloume, Abiogenic formation of alkanes in the Earth's crust as a minor source for global hydrocarbon reservoirs. *Nature* **416**, 522–524 (2002).
10. H. Chung, J. Gormly, R. Squires, Origin of gaseous hydrocarbons in subsurface environments: Theoretical considerations of carbon isotope distribution. *Chem. Geol.* **71**, 97–104 (1988).
11. A. A. Prinzhofer, A. Y. Huc, Genetic and post-genetic molecular and isotopic fractionations in natural gases. *Chem. Geol.* **126**, 281–290 (1995).
12. G. Proskurowski *et al.*, Abiogenic hydrocarbon production at lost city hydrothermal field. *Science* **319**, 604–607 (2008).
13. W. W. Carothers, Y. K. Kharaka, Aliphatic acid anions in oil-field waters—Implications for origin of natural gas. *AAPG Bull.* **62**, 2441–2453 (1978).
14. K. Kawamura, E. Tannenbaum, B. J. Huizinga, I. R. Kaplan, Volatile organic acids generated from kerogen during laboratory heating. *Geochem. J.* **20**, 51–59 (1986).
15. T. Barth, A. E. Borgund, A. L. Hopland, Generation of organic compounds by hydrous pyrolysis of Kimmeridge oil shale—Bulk results and activation energy calculations. *Org. Geochem.* **14**, 69–76 (1989).
16. V. B. Heuer *et al.*, Temperature limits to deep subseafloor life in the Nankai Trough subduction zone. *Science* **370**, 1230–1234 (2020).
17. T. Barth, Organic acids and inorganic ions in waters from petroleum reservoirs, Norwegian continental shelf: A multivariate statistical analysis and comparison with American reservoir formation waters. *Appl. Geochem.* **6**, 1–15 (1991).
18. P. Wellsbury *et al.*, Deep marine biosphere fuelled by increasing organic matter availability during burial and heating. *Nature* **388**, 573 (1997).
19. T. M. McCollom, J. S. Seewald, Experimental study of the hydrothermal reactivity of organic acids and acid anions: II. Acetic acid, acetate, and valeric acid. *Geochim. Cosmochim. Acta* **67**, 3645–3664 (2003).
20. B. Simoneit, P. Lonsdale, J. Edmond, W. C. Shanks III, Deep-water hydrocarbon seeps in Guaymas Basin, Gulf of California. *Appl. Geochem.* **5**, 41–49 (1990).
21. B. Simoneit, O. Kawka, Hydrothermal petroleum from diatomites in the Gulf of California. *Geol. Soc. Lond. Spec. Publ.* **26**, 217–228 (1987).
22. B. R. Simoneit, M. Mazurek, S. Brenner, P. Crisp, I. Kaplan, Organic geochemistry of recent sediments from Guaymas Basin, Gulf of California. *Deep-Sea Res. A, Oceanogr. Res. Pap.* **26**, 879–891 (1979).
23. J. Peter, P. Peltonen, S. Scott, B. Simoneit, O. Kawka, 14C ages of hydrothermal petroleum and carbonate in Guaymas Basin, Gulf of California: Implications for oil generation, expulsion, and migration. *Geology* **19**, 253–256 (1991).
24. B. M. Didyk, B. R. Simoneit, Hydrothermal oil of Guaymas Basin and implications for petroleum formation mechanisms. *Nature* **342**, 65 (1989).
25. B. R. Simoneit, E. M. Galimov, Geochemistry of interstitial gases in Quaternary sediments of the Gulf of California. *Chem. Geol.* **43**, 151–166 (1984).
26. B. R. Simoneit, O. Kawka, M. Brault, Origin of gases and condensates in the Guaymas Basin hydrothermal system (Gulf of California). *Chem. Geol.* **71**, 169–182 (1988).
27. C. S. Martens, Generation of short chain acid anions in hydrothermally altered sediments of the Guaymas Basin, Gulf of California. *Appl. Geochem.* **5**, 71–76 (1990).
28. K. L. Von Damm, J. M. Edmond, B. Grant, Chemistry of submarine hydrothermal solutions at Guaymas Basin, Gulf of California. *Geochim. Cosmochim. Acta* **49**, 2221–2237 (1985).
29. A. Teske, A. V. Callaghan, D. E. LaRowe, Biosphere frontiers of subsurface life in the sedimented hydrothermal system of Guaymas Basin. *Front. Microbiol.* **5**, 362 (2014).
30. A. Teske *et al.*, The Guaymas Basin hiking guide to hydrothermal mounds, chimneys, and microbial mats: Complex seafloor expressions of subsurface hydrothermal circulation. *Front. Microbiol.* **7**, 75 (2016).
31. S. Geilert *et al.*, On the formation of hydrothermal vents and cold seeps in the Guaymas Basin, Gulf of California. *Biogeosciences* **15**, 5715–5731 (2018).
32. A. Teske *et al.*, Microbial communities under distinct thermal and geochemical regimes in axial and off-axis sediments of Guaymas Basin. *Front. Microbiol.* **12**, 633649 (2021).
33. D. L. Williams, K. Becker, L. A. Lawver, R. P. Von Herzen, Heat flow at the spreading centers of the Guaymas Basin, Gulf of California. *J. Geophys. Res. Solid Earth* **84**, 6757–6769 (1979).
34. B. R. Simoneit, C. P. Summerhayes, P. A. Meyers, Sources and hydrothermal alteration of organic matter in Quaternary sediments: A synthesis of studies from the Central Gulf of California. *Mar. Pet. Geol.* **3**, 282–297 (1986).
35. L. McKay *et al.*, Thermal and geochemical influences on microbial biogeography in the hydrothermal sediments of Guaymas Basin, Gulf of California. *Environ. Microbiol. Rep.* **8**, 150–161 (2016).
36. A. Teske *et al.*, Microbial diversity of hydrothermal sediments in the Guaymas Basin: Evidence for anaerobic methanotrophic communities. *Appl. Environ. Microbiol.* **68**, 1994–2007 (2002).
37. T. Holler *et al.*, Thermophilic anaerobic oxidation of methane by marine microbial consortia. *ISME J.* **5**, 1946–1956 (2011).
38. O. Kniemeyer *et al.*, Anaerobic oxidation of short-chain hydrocarbons by marine sulphate-reducing bacteria. *Nature* **449**, 898–901 (2007).
39. R. Laso-Pérez *et al.*, Thermophilic archaea activate butane via alkyl-coenzyme M formation. *Nature* **539**, 396–401 (2016).
40. K. W. Seitz *et al.*, Asgard archaea capable of anaerobic hydrocarbon cycling. *Nat. Commun.* **10**, 1822 (2019).
41. J. F. Biddle *et al.*, Anaerobic oxidation of methane at different temperature regimes in Guaymas Basin hydrothermal sediments. *ISME J.* **6**, 1018–1031 (2012).
42. F. Widdel, O. Grundmann, "Biochemistry of the anaerobic degradation of non-methane alkanes" in *Handbook of Hydrocarbon and Lipid Microbiology,* K. N. Timmis, Ed. (Springer, 2010), pp. 909–924.
43. F. Dowell *et al.*, Microbial communities in methane-and short chain alkane-rich hydrothermal sediments of Guaymas Basin. *Front. Microbiol.* **7**, 17 (2016).
44. M. M. Adams, A. L. Hoarfrost, A. Bose, S. B. Joye, P. R. Girguis, Anaerobic oxidation of short-chain alkanes in hydrothermal sediments: Potential influences on sulfur cycling and microbial diversity. *Front. Microbiol.* **4**, 110 (2013).
45. R. Laso-Pérez *et al.*, Anaerobic degradation of non-methane alkanes by "*Candidatus* Methanoliparia" in hydrocarbon seeps of the Gulf of Mexico. *MBio* **10**, e01814–e01819 (2019).
46. C. J. Hahn *et al.*, "*Candidatus* Ethanoperedens," a thermophilic genus of *Archaea* mediating the anaerobic oxidation of ethane. *MBio* **11**, e00600–e00620 (2020).
47. I. M. Head, D. M. Jones, S. R. Larter, Biological activity in the deep subsurface and the origin of heavy oil. *Nature* **426**, 344–352 (2003).
48. X. Xia, J. Chen, R. Braun, Y. Tang, Isotopic reversals with respect to maturity trends due to mixing of primary and secondary products in source rocks. *Chem. Geol.* **339**, 205–212 (2013).
49. D. J. Des Marais, J. H. Donchin, N. L. Nehring, A. H. Truesdell, Molecular carbon isotopic evidence for the origin of geothermal hydrocarbons. *Nature* **292**, 826 (1981).
50. K. A. Kvenvolden, B. R. Simoneit, Hydrothermally derived petroleum: Examples from Guaymas Basin, Gulf of California, and Escanaba Trough, Northeast Pacific Ocean (1). *AAPG Bull.* **74**, 223–237 (1990).
51. A. M. Cruse, J. S. Seewald, Low-molecular weight hydrocarbons in vent fluids from the Main Endeavour Field, northern Juan de Fuca Ridge. *Geochim. Cosmochim. Acta* **74**, 6126–6140 (2010).
52. P. D. Jenden, B. R. T. Simoneit, R. P. Philp, "Hydrothermal effects on protokerogen of unconsolidated sediments from Guaymas Basin, Gulf of California: Elemental compositions, stable carbon isotope ratios and electron-spin resonance spectra" in *Initial Reports of the Deep Sea Drilling Project*, J. R. Curray *et al.*, Eds. (US Government Printing Office, Washington, DC, 1982), pp. 905–912.
53. D. McKirdy, T. Powell, Metamorphic alteration of carbon isotopic composition in ancient sedimentary organic matter: New evidence from Australia and South Africa. *Geology* **2**, 591–595 (1974).
54. S. G. Franks *et al.*, Carbon isotopic composition of organic acids in oil field waters, San Joaquin Basin, California, USA. *Geochim. Cosmochim. Acta* **65**, 1301–1310 (2001).
55. R. F. Dias, K. H. Freeman, M. D. Lewan, S. G. Franks, $\delta^{13}C$ of low-molecular-weight organic acids generated by the hydrous pyrolysis of oil-prone source rocks. *Geochim. Cosmochim. Acta* **66**, 2755–2769 (2002).
56. K. Von Damm *et al.*, The Escanaba Trough, Gorda Ridge hydrothermal system: Temporal stability and subseafloor complexity. *Geochim. Cosmochim. Acta* **69**, 4971–4984 (2005).
57. E. P. Reeves, J. M. McDermott, J. S. Seewald, The origin of methanethiol in midocean ridge hydrothermal fluids. *Proc. Natl. Acad. Sci. U.S.A.* **111**, 5474–5479 (2014).
58. A. Pearson, J. S. Seewald, T. I. Eglinton, Bacterial incorporation of relict carbon in the hydrothermal environment of Guaymas Basin. *Geochim. Cosmochim. Acta* **69**, 5477–5486 (2005).
59. D. R. Kester, I. W. Duedall, D. N. Connors, R. M. Pytkowicz, Preparation of artificial seawater 1. *Limnol. Oceanogr.* **12**, 176–179 (1967).
60. T. M. McCollom, J. S. Seewald, Experimental constraints on the hydrothermal reactivity of organic acids and acid anions: I. Formic acid and formate. *Geochim. Cosmochim. Acta* **67**, 3625–3644 (2003).
61. J. S. Seewald, M. Y. Zolotov, T. McCollom, Experimental investigation of single carbon compounds under hydrothermal conditions. *Geochim. Cosmochim. Acta* **70**, 446–460 (2006).
62. H. Olcay, L. Xu, Y. Xu, G. W. Huber, Aqueous-phase hydrogenation of acetic acid over transition metal catalysts. *ChemCatChem* **2**, 1420–1424 (2010).
63. T. N. Pham, T. Sooknoi, S. P. Crossley, D. E. Resasco, Ketonization of carboxylic acids: Mechanisms, catalysts, and implications for biomass conversion. *ACS Catal.* **3**, 2456–2473 (2013).
64. B. R. Brown, The mechanism of thermal decarboxylation. *Q. Rev. Chem. Soc.* **5**, 131–146 (1951).
65. C. R. Glein, I. R. Gould, E. D. Lorance, H. E. Hartnett, E. L. Shock, Mechanisms of decarboxylation of phenylacetic acids and their sodium salts in water at high temperature and pressure. *Geochim. Cosmochim. Acta* **269**, 597–621 (2020).

66. S. S. M. Konda, S. Caratzoulas, D. G. Vlachos, Computational insights into the role of metal and acid sites in bifunctional metal/zeolite catalysts: A case study of acetone hydrogenation to 2-propanol and subsequent dehydration to propene. *ACS Catal.* **6**, 123–133 (2016).
67. M. J. Antal, M. Carlsson, X. Xu, D. G. Anderson, Mechanism and kinetics of the acid-catalyzed dehydration of 1-and 2-propanol in hot compressed liquid water. *Ind. Eng. Chem. Res.* **37**, 3820–3829 (1998).
68. J. S. Seewald, Model for the origin of carboxylic acids in basinal brines. *Geochim. Cosmochim. Acta* **65**, 3779–3789 (2001).
69. L. J. McKay *et al.*, Spatial heterogeneity and underlying geochemistry of phylogenetically diverse orange and white Beggiatoa mats in Guaymas Basin hydrothermal sediments. *Deep Sea Res. Part I Oceanogr. Res. Pap.* **67**, 21–31 (2012).
70. V. Heuer *et al.*, Online $\delta^{13}C$ analysis of volatile fatty acids in sediment/porewater systems by liquid chromatography-isotope ratio mass spectrometry. *Limnol. Oceanogr. Methods* **4**, 346–357 (2006).
71. R. F. Aepfler, S. I. Bühring, M. Elvert, Substrate characteristic bacterial fatty acid production based on amino acid assimilation and transformation in marine sediments. *FEMS Microbiol. Ecol.* **95**, fiz131 (2019).
72. J. W. Pohlman, J. E. Bauer, W. F. Waite, C. L. Osburn, N. R. Chapman, Methane hydrate-bearing seeps as a source of aged dissolved organic carbon to the oceans. *Nat. Geosci.* **4**, 37 (2011).
73. Z. Cardman, "Active prokaryotic communities along a thermally and geochemically variable transect in Guaymas Basin hydrothermal sediments," MS thesis, University of North Carolina at Chapel Hill, Chapel Hill, NC (2014).